PHYSICAL REVIEW D **86,** 073009 (2012)

Higgs boson coupling sensitivity at the LHC using $H \to \tau\tau$ decays

Christopher Boddy,[1] Sinead Farrington,[2] and Christopher Hays[1]

[1] *University of Oxford, Oxford OX1 3RH, United Kingdom*

[2] *University of Warwick, Coventry CV4 7AL, United Kingdom*

(Received 3 August 2012; published 17 October 2012)

We investigate the potential for measuring the relative couplings of a low-mass Higgs boson at the Large Hadron Collider using WH, ZH, and $t\bar{t}H$ production, where the Higgs boson decays to tau-lepton pairs. With 100 fb^{-1} of $\sqrt{s} = 14$ TeV pp collision data we find that these modes can improve sensitivity to coupling-ratio measurements of a Higgs boson with a mass of about 125 GeV$/c^2$.

DOI: 10.1103/PhysRevD.86.073009 PACS numbers: 14.80.Bn

I. INTRODUCTION

The recent discovery [1] of a resonance with a mass of about 125 GeV [2] in pp collisions at the Large Hadron Collider (LHC) could well correspond to the long-awaited observation of the Higgs boson [3] of the standard model (SM). If so, it would herald another remarkable success of the SM, which predicted the existence of a Higgs boson with a mass less than 152 GeV at 95% confidence level (C.L.) [4] based on precision measurements of electroweak parameters such as the masses of the W [5] and Z [6] bosons, and of the top quark [7].

While the observed properties of the new resonance are consistent with those of the SM Higgs boson, further measurements are required to determine if it has one of the key properties predicted by the SM: couplings to fermions that are proportional to their masses. Fortunately, a Higgs boson with a mass of 125 GeV provides a wealth of decay modes in which to study its couplings. In addition to the subleading decays that dominate the sensitivity of the initial observation ($H \to \gamma\gamma$, $H \to ZZ$, and $H \to WW$), the leading decays $H \to b\bar{b}$ and $H \to \tau\tau$ can be observed in various production processes [8–11]. As a result, a wide variety of Higgs boson cross section measurements will provide incisive tests of specific SM couplings [12,13].

The prospects for Higgs boson discovery and measurement have been studied extensively [14]; however, low-rate processes observable with the full LHC design luminosity have not been completely explored. We investigate the sensitivity of 100 fb^{-1} of $\sqrt{s} = 14$ TeV LHC data to the Higgs boson production processes WH, ZH, and $t\bar{t}H$, followed by $H \to \tau\tau$ and at least one $W \to l\nu$ or $Z \to ll$ decay [15]. The potential measurement sensitivity to the WH process has been considered only perfunctorily [16], though the CMS experiment has recently performed the first WH search in the $H \to \tau\tau$ decay channel at the LHC [17]. Studies of $t\bar{t}H$ production have been performed in various top-quark and tau-lepton decay channels [18,19]; we revisit $t\bar{t} + H(\to \tau\tau)$ production in light of the demonstrated performance of the ATLAS and CMS experiments in separating hadronic tau decays from the large hadronic jet background in data [20]. Combining the prospects for measurements of associated Higgs boson production in the $\tau\tau$ decay channel with those in the $b\bar{b}$ decay channel [8–10] improves the expected LHC sensitivity to the Yukawa coupling ratio $g_{Hbb}/g_{H\tau\tau}$. This ratio is determined at tree level by the bottom-quark and tau-lepton masses and is thus sensitive to differences in the source of mass for quarks and leptons [21]. The ratios of associated Higgs production measurements also directly provide the coupling ratios g_{Htt}/g_{HWW} and g_{HWW}/g_{HZZ}.

This paper is structured as follows: Section II outlines the procedures for generating, simulating and selecting Higgs boson and background events; Sec. III describes the specific selection and expected signal and background yields for the WH, ZH, and $t\bar{t}H$ processes; Sec. IV presents the results of the fit to cross section in each channel and the uncertainties on partial-width ratios; and Sec. V summarizes our conclusions.

II. SIGNAL AND BACKGROUND SIMULATION

We simulate all signal and background processes using the SHERPA [22] event generator, except for $W + 6$ jets, which is simulated using ALPGEN [23] for the hard process and PYTHIA [24] for the hadronization and showering. The $W + 6$ jets and $t\bar{t} + 2$ jets cross sections are obtained from ALPGEN; all other processes are normalized to cross sections calculated at next-to-leading order (NLO) in α_s. Detector resolutions and efficiencies are modelled using the DELPHES simulation [25] with corrections based predominantly on ATLAS [26] performance projections; similar performance is expected with the CMS [27] detector. Events are selected using the reconstructed DELPHES objects.

A. Event generation and cross sections

We use CTEQ6M parton distribution functions [28] for cross section calculations. Samples are generated with quark and gluon jets included to leading order at the matrix-element level, and additional jets modelled by parton showering. Tau leptons are decayed within SHERPA.

The cross sections and branching ratios for the Higgs boson production and decay processes are shown in

TABLE I. Higgs boson production cross sections [29,30] and branching ratios [31] as a function of m_H.

m_H (GeV)	$\sigma(pp \to WH)$	$\sigma(pp \to ZH)$	$\sigma(pp \to t\bar{t}H)$	BR($H \to \tau\tau$)
115	1.98 pb	1.05 pb	0.785 pb	0.0739
120	1.74 pb	0.922 pb	0.694 pb	0.0689
125	1.53 pb	0.813 pb	0.623 pb	0.0620
130	1.35 pb	0.718 pb	0.559 pb	0.0537
135	1.19 pb	0.638 pb	0.501 pb	0.0444

Table I. We study Higgs boson masses (m_H) in the 115–135 GeV range to investigate the dependence of the expected sensitivity on m_H. Cross sections for $W/Z + H$ production are calculated with V2HV [29] and include QCD corrections at NLO. The next-to-next-to-leading order QCD [32] and NLO electroweak [33] corrections are $\lesssim 5\%$ relative to the V2HV calculation. Cross sections for $t\bar{t}H$ production include QCD corrections at NLO [30]. The uncertainties on all signal cross sections are $\mathcal{O}(10\%)$, while those on the branching ratios determined from HDECAY [31] are $\mathcal{O}(1\%)$.

The dominant backgrounds to the $W/Z + H$ processes are the production of dibosons, where the bosons decay leptonically, and $W/Z +$ hadronic jet(s), $t\bar{t}$, and tW, where at least one jet is (mis)reconstructed as a lepton. Background production cross sections are obtained from MCFM [34] and, for $t\bar{t}$, an NLO plus next-to-leading log (NLL) calculation [35]. For the $W/Z +$ jets backgrounds, we calculate cross sections requiring the boson mass to be between 20 and 200 GeV, the jets to have $p_T > 15$ GeV and $|\eta| < 3.5$, and, when there are two or more jets, $m_{jj} >$ 20 GeV. The cross sections multiplied by SM branching ratios [36] are shown in Table II.

The $t\bar{t}H$ process, with $H \to \tau\tau$, has relatively little background. The irreducible background $t\bar{t}Z$ has a cross section [37] that is lower than the signal process. The background where hadronic jets are (mis)reconstructed as leptons results predominantly from $t\bar{t}$ production in association with 2 or 3 jets. We estimate this background using a leading-order cross section calculated with ALPGEN [23]. The calculation requires jets with $p_T > 15$ GeV and $|\eta| < 3.5$, and $\Delta R > 0.7$ between jets. The potential background of $W + 6$ jets production is studied using an ALPGEN cross section with the above jet requirements and the W boson mass between 50 and 120 GeV. We find it to be negligible.

TABLE II. Background production cross sections obtained from ALPGEN [23] ($W + 6$ jets and $t\bar{t} + 2$ jets), an NLO plus NLL calculation ($t\bar{t}$ [35]), and MCFM [34] (the remaining processes), multiplied by SM branching ratios [36]. In this table l represents e, μ or τ.

Production process	Cross section $\times$ BR
$W(\to l\nu)Z/\gamma^*(\to ll)$	52.4 pb $\times$ 3.27% = 1.56 pb
$Z/\gamma^*(\to ll)Z/\gamma^*(\to \tau\tau)$	17.7 pb $\times$ 0.340% = 60.2 fb
$W(\to l\nu) + 2$ jets	26 772 pb $\times$ 32.4% = 8674 pb
$Z/\gamma^*(\to ll) + 1$ jet	24 466 pb $\times$ 10.1% = 2471 pb
$Z/\gamma^*(\to ll) + 2$ jets	9018 pb $\times$ 10.1% = 911 pb
$W(\to l\nu) + 6$ jets	23.5 pb $\times$ 32.4% = 7.61 pb
$t\bar{t}(\to l\nu l\nu b\bar{b})$	933 pb $\times$ 10.5% = 97.9 pb
$t\bar{t}(\to l\nu q\bar{q}b\bar{b}) + 2$ jets	255 pb $\times$ 43.8% = 112 pb
$t\bar{t}(\to l\nu l\nu b\bar{b}) + 2$ jets	255 pb $\times$ 10.5% = 26.8 pb
$tW(\to l\nu bl\nu)$	61.8 pb $\times$ 10.5% = 6.49 pb
$t\bar{t}(\to l\nu q\bar{q}b\bar{b})Z/\gamma^*(\to ll)$	973 fb $\times$ 4.34% = 42.2 fb

B. Detector simulation

We model detector acceptance and response using the DELPHES simulation program [25]. The detector consists of a charged-particle tracker covering $|\eta| < 2.5$ surrounded by a calorimeter with coverage to $|\eta| = 4.9$. The calorimeter has a granularity of $\Delta\eta \times \Delta\phi = 0.1 \times 0.1$ and is divided into central ($|\eta| < 1.7$), forward ($1.7 < |\eta| < 3.2$), and endcap ($3.2 < |\eta| < 4.9$) regions with separate resolutions. Additional segmentation into electromagnetic and hadronic calorimeters provides improved resolution for electrons and photons relative to hadrons.

Detector resolutions are modelled by smearing the reconstructed momentum with a Gaussian resolution. Muon resolution is parametrized as $\sigma(p_T)/p_T = 1\%$, which is the approximate expected resolution of muons from weak boson decays [38]. Calorimeter resolutions are parametrized as

$$\frac{\sigma_E}{E} = C \oplus \frac{S}{\sqrt{E}} \oplus \frac{N}{E},$$

where E is expressed in units of GeV. In the central and forward electromagnetic calorimeters the only significant term applied is a sampling term S of about $10\%\sqrt{\mathrm{GeV}}$. The resolution of the hadronic calorimeters is also dominated by the sampling term, which ranges from about 50% in the central region to $\approx 95\%$ in the endcap region. The constant terms C provide small additional contributions of about 3% and 7.5% in the central and endcap regions respectively. The sampling and constant terms in the forward region are roughly in the middle of the corresponding central and endcap terms. The noise term (N/E) is negligible for the final states we consider.

The detector acceptance for electrons, tau leptons, and charged-particle tracks is assumed to be $|\eta| < 2.5$. Muon coverage is assumed to extend to $|\eta| < 2.7$. Because of the potential challenges in reconstructing jets in the forward region at high luminosity, we conservatively assume a jet acceptance of $|\eta| < 3.5$. Jets are reconstructed with the anti-k_t algorithm [39] with cone radius 0.4. Hadronic tau decays are identified as jets with >90% of their energy within a cone of $\Delta R < 0.15$ and only one reconstructed track with $p_T > 2$ GeV and $\Delta R < 0.4$ from the jet axis. Electrons and muons are identified if no additional track with $p_T > 2$ GeV lies within a cone of $\Delta R < 0.2$ from the e or μ. Finally, the p_T imbalance in the event ($\not{p}_T$) is derived by summing over the momentum of each calorimeter tower and muon. Muons deposit no energy in the calorimeter in DELPHES.

Efficiencies are applied to leptons according to the expected ATLAS performance [26] or, for τ identification, the ATLAS detector performance from 2011 data [20] (Table III). Trigger efficiencies are based on a trigger requiring a single electron or muon with $p_T > 25$ GeV. While actual thresholds may be higher, the presence of multiple leptons should allow a set of triggers with a similar combined efficiency. Rates for hadronic jets to be misidentified as leptons are also based on expected ATLAS performance and are shown in Table III. Since we always consider electrons and muons together, the averages of e and μ efficiencies and misidentification rates are the relevant quantities (rather than the individual rates).

The $\not{p}_T$ resolution is expected to degrade from additional interactions present at the design luminosity of $\mathcal{L} = 10^{-34}$ cm^{-2} s^{-1}. At this luminosity and 25 ns bunch spacing, one can expect ≈ 25 interactions per crossing. Each interaction will deposit $\sum E_T \approx 30$ GeV in the calorimeter, and the $\not{p}_T$ resolution is expected to be $\approx 0.5\sqrt{\sum E_T}$ [26]. To account for the degradation in $\not{p}_T$ resolution from the additional interactions, we add a Gaussian resolution with $\sigma = 15$ GeV to the projections $\not{p}_x$ and $\not{p}_y$.

The performance of τ_h identification at $\sqrt{s} = 14$ TeV in the presence of 25 additional interactions is difficult to predict. In addition to our nominal efficiency of 30%, we study an optimistic scenario where the efficiency is increased to 40% for the same misidentification rate. The two scenarios give an indication of the effect of the performance of tau identification on the results.

TABLE III. Lepton trigger and identification efficiencies, and rates for hadronic jets to be misidentified as leptons. Efficiencies and misidentification rates are applied to objects at the generator level.

Object	Efficiency (%)		Misidentification rate (%)
	Trigger	Identification	
e/μ	87	79	0.085
τ_h	...	30	1.0

III. EVENT SELECTION

Each of the three production channels (WH, ZH and $t\bar{t}H$) is subdivided according to the decay of the tau leptons originating from the Higgs boson. The general strategy is to define a simple cut-based selection for each decay channel and then to perform a one-dimensional likelihood fit to a mass-based distribution. The simple selection limits the number of assumptions on the detector performance; the key assumptions are relatively low jet-to-τ_h misreconstruction rates and reasonable $\not{p}_T$ resolution. The fit reduces the effect of normalization uncertainties on the background. We assume that the dominant uncertainties will result from extrapolations of control regions in data, and will not significantly affect the sensitivity.

A. WH selection

Considering only the leptonic W-boson decays, the WH final state contains one lepton, $\not{p}_T$ from the neutrino, and two tau leptons from the Higgs boson decay. Events where at least two τ leptons decay hadronically are not included in this study because the $\approx 1\%$ jet-to-τ_h misidentification rate leads to overwhelming background from W + jets production. Events where all tau leptons decay leptonically are also not included because the relatively low branching ratio results in marginal sensitivity in the corresponding final state; adding it to the final state with one τ_h would reduce the uncertainty on the WH cross section by $\approx 20\%$. We study the final state $l_W \tau_l \tau_h \not{p}_T$, where l_W is an e or μ assumed to come from a W-boson decay and τ_l is an e or μ assumed to come from a tau-lepton decay. We define l_W by $p_T^{l_W} > p_T^{\tau_l}$; in more than 80% of signal events the lepton from the W boson decay has higher p_T than that from the tau-lepton decay.

There are several background contributions to the $l_W \tau_l \tau_h \not{p}_T$ final state. Production of W and Z bosons in association with hadronic jets, as well as $t\bar{t}$ and tW decays, contribute when at least one hadronic jet is misreconstructed as a lepton. We model these backgrounds by applying the hadronic misidentification rates listed in Table III to all jets in the events. Production of WZ background and WH signal are modelled using Monte Carlo (MC) acceptances, with corrections for trigger and identification efficiencies (Table III).

The presence of neutrinos from the τ-lepton and W-boson decays prevents a full reconstruction of the Higgs boson mass. However, the "visible mass," defined as the invariant mass of the $\tau_l \tau_h$ pair, is correlated with the Higgs boson mass. We perform a likelihood fit to the visible mass distribution to extract the signal yield.

Event selection begins with the reconstructed objects in the final state. For the signal process, an e or μ from the W-boson decay typically has the highest p_T of the three charged leptons, with a p_T distribution that peaks around 40 GeV. We therefore require $p_T^{l_W} > 25$ GeV. The unobserved neutrinos in tau-lepton decays reduce the p_T of the reconstructed objects, so a p_T threshold of 15 GeV is applied to τ_l and τ_h. Background from W + jets is suppressed by requiring the charges of the leptons (q_l) to sum to ± 1. Events are required to have no jet with $p_T >$ 25 GeV and $|\eta| < 3.5$, reducing both top-quark and W/Z + jets backgrounds. A requirement of $\not{p}_T >$ 30 GeV reduces background from Z + jet production, and an upper bound of $\not{p}_T < 80$ GeV reduces top-quark background.

The significant background from $Z(\to \tau\tau)$ + jet production contributes primarily when the tau leptons decay leptonically and the jet is misreconstructed as a τ_h. Each tau lepton from the Z boson decay is highly boosted and its decay products are nearly collinear. In a class of Z + jet events, the reconstructed $\not{p}_T$ is aligned with l_W, while in signal events the $\not{p}_T$ is rarely aligned with l_W. Defining the transverse mass as $m_T = \sqrt{2(p_T^{l_W}\not{p}_T - p_x^{l_W}\not{p}_x - p_y^{l_W}\not{p}_y)}$, we suppress Z + jet events with the requirement $m_T >$ 50 GeV. Additional background rejection could be achieved with a similar transverse mass requirement on τ_l and $\not{p}_T$; however, there would be larger reduction in signal since there are neutrinos collinear with τ_l in signal events.

A final selection requirement of no opposite-charge, same-flavor $l_W\tau_l$ further reduces background from Z + jet production, removing most events with Z bosons decaying to e or μ pairs. Decays of Z bosons to tau-lepton pairs are also reduced with this requirement, and could be further reduced by removing events with an oppositely charged electron and muon. However, the loss of signal from such a requirement would be relatively large, and the statistical sensitivity would degrade.

Figure 1 shows the $\not{p}_T$, m_T and $m(\tau_h\tau_l)$ distributions with all selection requirements applied, except those on the plotted quantity. The numbers of signal (N_s^{WH}) and background (N_b^{WH}) events, as well as $N_s^{WH}/\sqrt{N_b^{WH}}$, are given in Table IV after each selection requirement. The detailed contribution of each background and the dependence of the signal yield on m_H are shown after all selection in Tables V and VI, respectively.

The selection gives modest statistical sensitivity to WH production, but the sensitivity is improved with a fit to the visible mass distribution. Normalization uncertainties will be mitigated by this fit, though uncertainties on the shape of the visible mass distribution are also relevant; we assume the systematic uncertainties can be sufficiently constrained by studying independent kinematic regions (for example, the high-$\not{p}_T$ region for top production, and the low-m_T region for Z + jet production).

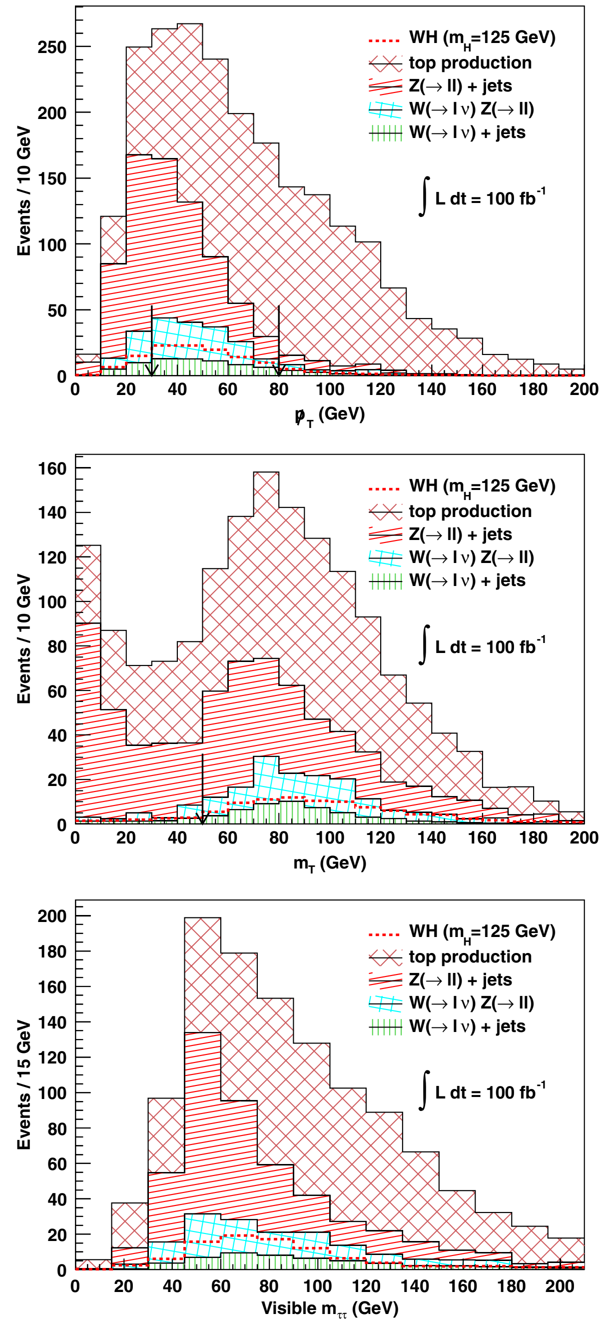

FIG. 1 (color online). The $\not{p}_T$ (top), m_T (middle) and $m(\tau_h\tau_l)$ distributions after all $l_W\tau_l\tau_h\not{p}_T$ selection requirements, except for requirements on the plotted distribution. The selected regions are between the arrows in the $\not{p}_T$ plot and above the arrow in the m_T plot. Shown are the WH signal (dashed line) and the following backgrounds: top-quark (diagonal-hatched region), Z + jet (tilted-lined region), WZ (tilted-hatched region), and W + jet (vertical-lined region) production.

B. ZH selection

In contrast to WH production, $ZH \to ll\tau\tau$ production is dominated by an irreducible background (ZZ), with relatively low signal statistics in 100 fb^{-1} of integrated luminosity. Thus, the selection strategy is to apply few requirements and to combine the $l_Z l_Z \tau_h\tau_h$ and $l_Z l_Z \tau_h\tau_l$ decay channels, where l_Z is an e or μ. The $l_Z l_Z \tau_l\tau_l$ channel

TABLE IV. The numbers of WH signal and background events passing each set of requirements, for an integrated luminosity of 100 fb^{-1} and $m_H = 125$ GeV. Also shown is the signal over the square root of background, a measure of the statistical sensitivity to the signal. Additional sensitivity is gained from a fit to the visible mass distribution.

Selection	N_s^{WH}	N_b^{WH}	$N_s^{WH}/\sqrt{N_b^{WH}}$
$p_T^{l_W} > 25$ GeV, $p_T^{\tau_l,\tau_h} > 15$ GeV, $\sum q_l = \pm 1$ and no jet	233	171408	0.6
$30 < \not{p}_T < 80$ GeV	137	19124	1.0
$m_T > 50$ GeV	103	1582	2.6
No opposite-sign same-flavor $l_W\tau_l$	92	1177	2.7

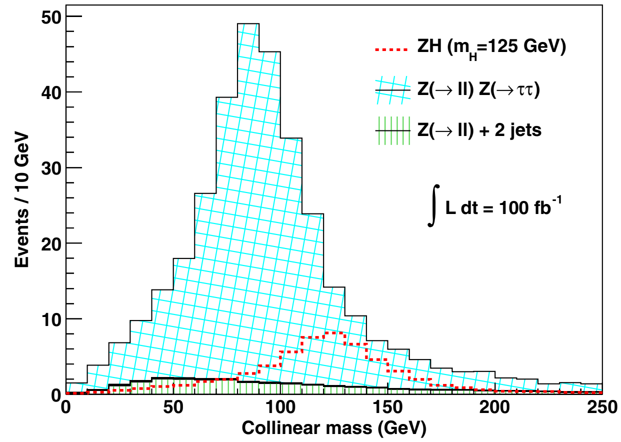

FIG. 2 (color online). The collinear mass distribution for the ZH signal (dashed line), ZZ background (tilted-hatched region), and $Z + 2$ jets background (vertical-lined region). Not shown is the negligible $t\bar{t}$ background.

TABLE V. The contribution of each background to the $l_W\tau_l\tau_h\not{p}_T$ final state for an integrated luminosity of 100 fb^{-1}.

Process	Number of events
$t\bar{t}(\rightarrow l\nu l\nu b\bar{b})$	573
$Z/\gamma^*(\rightarrow ll) + 1$ jet	330
$tW(\rightarrow l\nu bl\nu)$	112
$W(\rightarrow l\nu)Z/\gamma^*(\rightarrow \tau\tau)$	81
$W(\rightarrow l\nu) + 2$ jets	52
$W(\rightarrow l\nu)Z/\gamma^*(\rightarrow ee/\mu\mu)$	30
Total	1177

TABLE VIII. The contribution of each background to the ZH final state for an integrated luminosity of 100 fb^{-1}.

Process	Number of events
$Z/\gamma^*(\rightarrow ll)Z/\gamma^*(\rightarrow \tau\tau)$	305
$Z/\gamma^*(\rightarrow ll) + 2$ jets	25
$t\bar{t}(\rightarrow l\nu l\nu b\bar{b})$	2
Total	332

TABLE VI. The number of WH signal events for m_H in the range 115–135 GeV, and the statistical significance of the excess of signal events over background in 100 fb^{-1} of integrated luminosity.

m_H(GeV)	N_s^{WH}	$N_s^{WH}/\sqrt{N_b^{WH}}$
115	122	3.6
120	109	3.2
125	92	2.7
130	70	2.0
135	52	1.5

TABLE IX. The number of ZH signal events for m_H in the range 115–135 GeV, and the statistical significance of the excess of signal events over background in 100 fb^{-1} of integrated luminosity.

m_H(GeV)	N_s^{ZH}	$N_s^{ZH}/\sqrt{N_b^{ZH}}$
115	77	4.2
120	71	3.9
125	56	3.1
130	45	2.4
135	33	1.8

TABLE VII. The numbers of ZH signal and background events passing each set of requirements, for an integrated luminosity of 100 fb^{-1} and Higgs boson mass of 125 GeV. Also shown is the signal over the square root of background, a measure of the statistical sensitivity to the signal. Additional sensitivity is gained from a fit to the collinear mass distribution.

Selection	N_s^{ZH}	N_b^{ZH}	$N_s^{ZH}/\sqrt{N_b^{ZH}}$
Opposite-charge $\tau_h\tau_h$ and l_Zl_Z; highest (lowest) $p_T^{l_Z} > 25(15)$ GeV; $p_T^{\tau_h} > 25$ GeV	32	193	2.3
Collinear mass solution	26	144	2.1
Opposite-charge $\tau_h\tau_l$ and l_Zl_Z; highest (lowest) $p_T^{l_Z} > 25(15)$ GeV; $p_T^{\tau_h(\tau_l)} > 25(15)$ GeV	36	266	2.2
Collinear mass solution	30	188	2.2

adds only marginal sensitivity because of the small branching ratio and the increased ZZ background.

In addition to the irreducible $ZZ \to ll\tau\tau$ background, reducible backgrounds from Z + jets and $t\bar{t} \to l\nu l\nu b\bar{b}$ contribute when two jets are misreconstructed as hadronic tau and/or light-flavor lepton(s). These backgrounds are modelled by applying the hadronic misidentification rates in Table III to MC-generated events. Production of ZZ background and ZH signal are modelled using trigger- and identification-corrected MC acceptances (Table III).

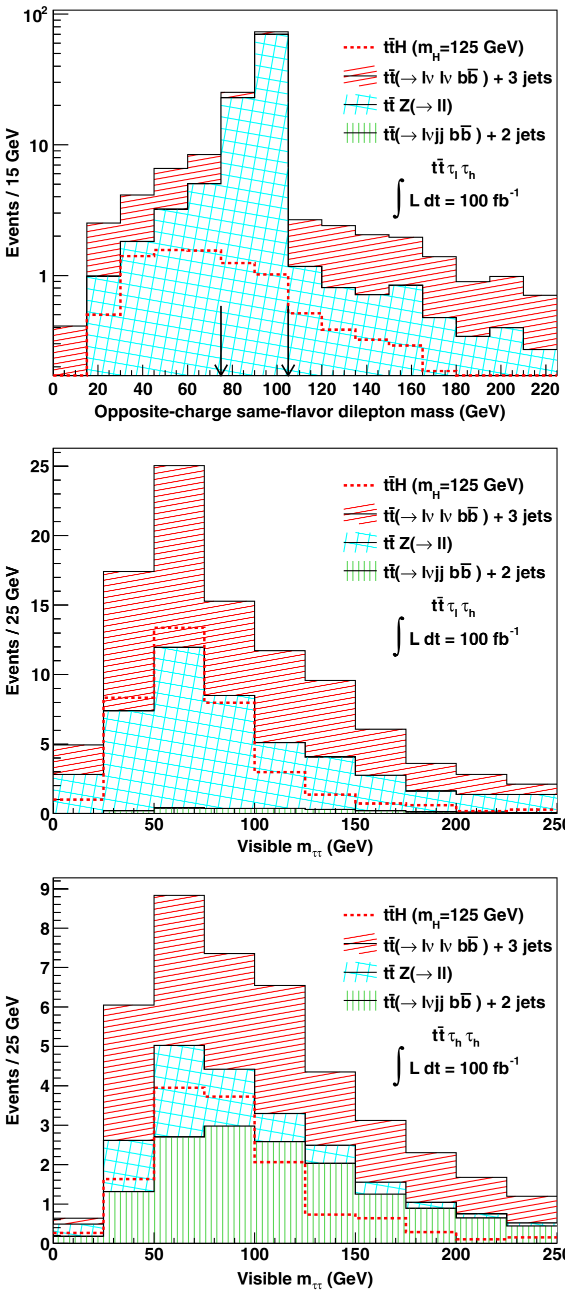

FIG. 3 (color online). The $m(l_W\tau_l)$ (top), $m(\tau_h\tau_l)$ (middle), and $m(\tau_h\tau_h)$ distributions after all selection requirements [except for the requirement on $m(l_W\tau_l)$ for the $m(l_W\tau_l)$ distribution]. The selected $m(l_W\tau_l)$ regions are below and above the arrows in the $m(l_W\tau_l)$ plot. Shown are the $t\bar{t}H$ signal (dashed line) and the following backgrounds: $t\bar{t}$ + 3 jets (tilted-lined region), $t\bar{t} + Z$ (tilted-hatched region), and $t\bar{t}$ + 2 jets (vertical-lined region) production.

The irreducible ZZ background can be separated using the invariant mass of the tau-lepton pair. Since the tau leptons from the Higgs boson decay are highly boosted, their decay products are nearly collinear. Assuming collinear tau-lepton decays, the net neutrino momentum from each decay can be resolved. The resulting invariant mass of the tau-lepton pair, or "collinear mass", can be expressed in the $ll\tau_h\tau_l$ decay channel as $m(\tau_h, \tau_l)/\sqrt{\chi_h\chi_l}$, where $\chi_{h(l)}$ is the fraction of tau-lepton energy taken by $\tau_h(\tau_l)$. The fractions χ_h and χ_l can be solved in terms of measured quantities,

$$\chi_h = \frac{p_x^{\tau_h}p_y^{\tau_l} - p_y^{\tau_h}p_x^{\tau_l}}{p_x^{\tau_h}p_y^{\tau_l} + \not{p}_x p_y^{\tau_l} - p_y^{\tau_h}p_x^{\tau_l} - \not{p}_y p_x^{\tau_l}},$$
$$\chi_l = \frac{p_x^{\tau_h}p_y^{\tau_l} - p_y^{\tau_h}p_x^{\tau_l}}{p_x^{\tau_h}p_y^{\tau_l} + \not{p}_x p_y^{\tau_h} - p_y^{\tau_h}p_x^{\tau_l} - \not{p}_y p_x^{\tau_h}}. \quad (1)$$

For the $ll\tau_h\tau_h$ channel, τ_l is replaced by the other τ_h. We fit the collinear mass distribution to extract the ZH signal yield after initial selection requirements.

The selection requires two opposite-charge same-flavor leptons from the Z boson decay. If an event has multiple candidate pairs, we define the pair with invariant mass closest to m_Z as the Z boson candidate decay. The highest (lowest) p_T lepton from the decay is required to have $p_T > 25(15)$ GeV. We then require two opposite-charge tau-lepton decay candidates with $p_T > 25$ GeV (or $p_T >$ 15 GeV for τ_l). Table VII shows the numbers of signal (N_s^{ZH}) and background (N_b^{ZH}) events, as well as $N_s^{ZH}/\sqrt{N_b^{ZH}}$, in each channel after this initial selection. The collinear mass requirement reduces the signal yield by nearly 30%; recovering these events with an alternative mass variable would improve the measurement.

Figure 2 shows the collinear mass distribution with all selection requirements. The detailed contribution of each background and the dependence of the signal yield on m_H are shown after all selection requirements in Tables VIII and IX, respectively. The relatively small background and the discrimination given by the collinear mass make the

TABLE X. The contribution of each background to the $t\bar{t}H$ final states for an integrated luminosity of 100 fb^{-1}.

Process	$t\bar{t} + \tau_h\tau_l$	$t\bar{t} + \tau_h\tau_h$
$t\bar{t}(\to l\nu l\nu b\bar{b})$ + 3 jets	52	20
$t\bar{t}(\to l\nu q\bar{q}b\bar{b}) + Z/\gamma^*(\to ee/\mu\mu)$	32	2
$t\bar{t}(\to l\nu q\bar{q}b\bar{b}) + Z/\gamma^*(\to \tau\tau)$	13	5
$t\bar{t}(\to l\nu q\bar{q}b\bar{b})$ + 2 jets	2	15
Total	99	42

TABLE XI. The number of $t\bar{t}H$ signal events in each channel for m_H in the range 115–135 GeV, and the statistical significance of the excess of signal events over background in 100 fb^{-1} of integrated luminosity. The $t\bar{t}$ pair is selected in the $l_W \nu q\bar{q}b\bar{b}$ final state.

m_H(GeV)	Channel	N_s^{ttH}	$N_s^{ttH}/\sqrt{N_b^{ttH}}$
115	$t\bar{t}+\tau_h\tau_l$	47	4.8
	$t\bar{t}+\tau_h\tau_h$	17	2.7
120	$t\bar{t}+\tau_h\tau_l$	47	4.8
	$t\bar{t}+\tau_h\tau_h$	16	2.5
125	$t\bar{t}+\tau_h\tau_l$	37	3.7
	$t\bar{t}+\tau_h\tau_h$	14	2.1
130	$t\bar{t}+\tau_h\tau_l$	30	3.0
	$t\bar{t}+\tau_h\tau_h$	11	1.7
135	$t\bar{t}+\tau_h\tau_l$	22	2.2
	$t\bar{t}+\tau_h\tau_h$	7	1.1

ZH channel particularly promising for measuring Higgs boson decays to tau leptons.

C. $t\bar{t}H$ selection

The cross section for $t\bar{t}H$ production, with the Higgs boson decaying to tau leptons, is relatively low. We focus on the decays with the highest branching ratios, excluding fully hadronic $t\bar{t}$ decays because of the potentially large multijet background. Thus we consider $t\bar{t} \to l_W \nu q\bar{q}b\bar{b}$ and either $H \to \tau_h\tau_h$ or $H \to \tau_l\tau_h$, with l_W defined by $p_T^{l_W} > p_T^{\tau_l}$. These final states are the same as in WH production but with the addition of four jets.

For the detector performance assumed in Sec. II B, the background is a roughly equal mix of irreducible $t\bar{t}Z$ production and reducible $t\bar{t}$ + jets production. The dominant reducible background is $t\bar{t}(\to l_W \nu l \nu b\bar{b})$ + 3 jets, where one jet is misreconstructed as a τ_h, and l is identified as either τ_h or τ_l. The generation of $t\bar{t}$ + 3 jets at tree level is computationally intensive; we therefore model this background using the SHERPA $t\bar{t}$ + 2 jets process, with additional jets modelled by the SHERPA parton-showering algorithm.

Since the reducible background consists of $t\bar{t}$ + jets, the sensitivity depends predominantly on tau identification and the broadly peaking visible mass distribution of the tau-lepton pair. The irreducible $t\bar{t}Z$ background is suppressed by requiring opposite-sign same-flavor $l_W\tau_l$ pairs to have an invariant mass outside the 75–105 GeV peak of resonant Z-boson production. Other selection requirements are $p_T^{l_W} > 25$ GeV, $p_T^{\tau_h,\tau_l} > 15$ GeV, $\sum q_\ell = \pm 1$, and at least 4 jets.

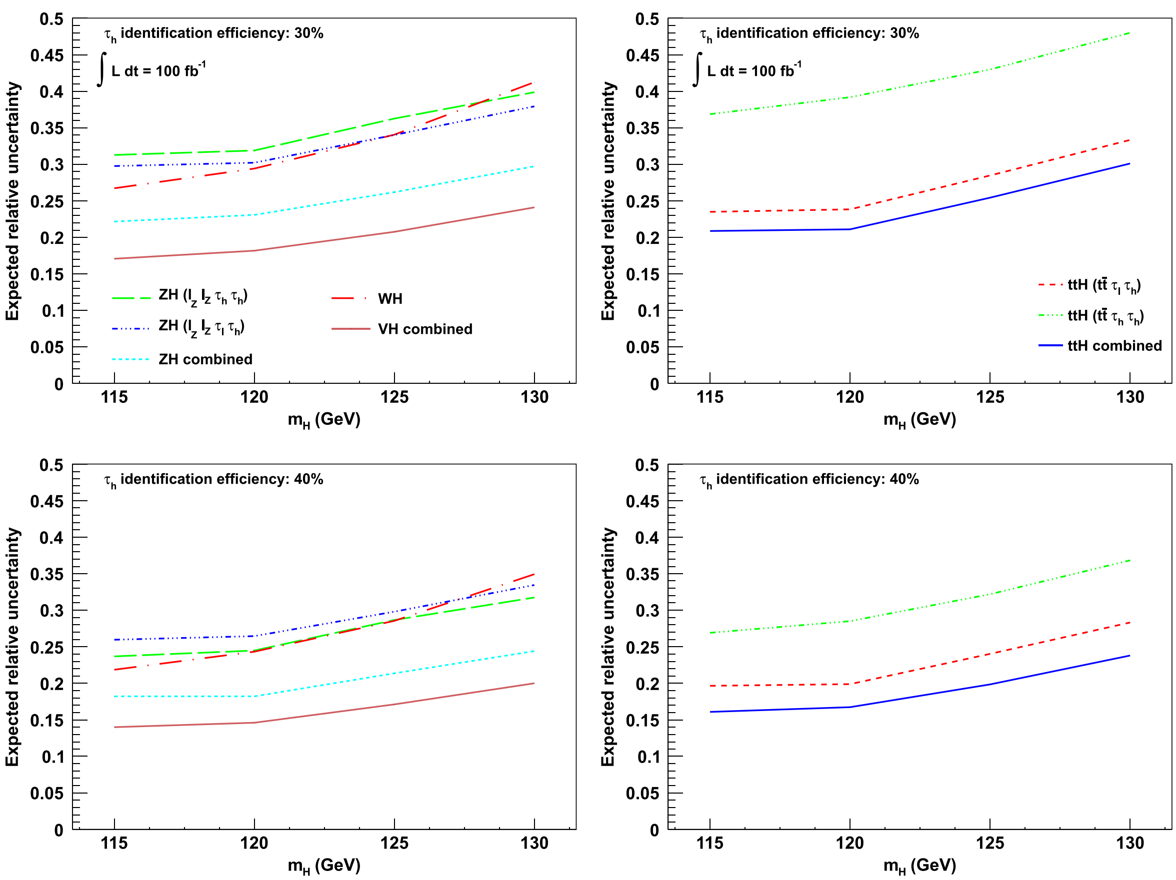

FIG. 4 (color online). The expected relative statistical uncertainties on $\sigma \times$ BR of VH (left, $V = W, Z$) and $t\bar{t}H$ (right) production for the nominal (top) and optimistic (bottom) tau identification performance scenarios.

TABLE XII. The assumed relative uncertainties on $V(H \rightarrow b\bar{b})$ and $t\bar{t}(H \rightarrow b\bar{b})$ [9] cross section measurements in data corresponding to 100 fb^{-1} of integrated luminosity.

m_H(GeV)	VH (%)	$t\bar{t}H$ (%)
115	10	19
120	12	22
130	17	34

Figure 3 shows the mass distribution of opposite-sign same-flavor $l_W \tau_l$ pairs and the visible mass distributions of the tau-lepton pairs in the two decay channels $t\bar{t} + \tau_h \tau_l$ and $t\bar{t} + \tau_h \tau_h$. Tables X and XI, respectively, show the contribution of each background and the dependence of the signal yield on m_H after all selection for both channels. With basic object selection, reasonable sensitivity to $t\bar{t}H$ production can be obtained if tau leptons are identified with a similar efficiency and jet rejection rate to that achieved by ATLAS and CMS with $\sqrt{s} = 7$ TeV LHC data.

IV. RESULTS

We determine the expected sensitivity to the cross section of a given process using pseudoexperiments [15]. In each pseudoexperiment, data are produced according to a Poisson distribution in each bin of the relevant mass-based fit distribution, where the mean of the Poisson is equal to the combined signal and background in that bin. The number of signal events is determined by minimizing the negative log likelihood of the fit distribution. This procedure is performed for 10^4 pseudoexperiments for each process, and the uncertainty is taken to be the root-mean square of the resulting signal-yield distribution. The relative statistical uncertainties on $\sigma \times$ BR of the signal processes are shown in Fig. 4.

The cross section of a given signal process includes the product of partial widths for the production and decay vertices of the Higgs boson. Individual partial widths can be determined by taking cross section ratios, providing direct access to the individual couplings of the Higgs boson to SM particles. We expect this procedure to provide the additional benefit of cancelling many experimental uncertainties. From the ratios of cross section measurements studied in this paper, and from the expected uncertainties on the measurements of associated Higgs production in its decays to bottom quarks (Table XII), we obtain the expected sensitivity to partial-width ratios shown in Fig. 5.

V. CONCLUSIONS

With the recent discovery of a resonance with cross sections consistent with that of the SM Higgs boson, tests of the specific SM predictions of the Higgs boson couplings are a high priority. A Higgs boson with a mass of 125 GeV can be measured in a wealth of production and decay channels. We have performed a detailed study of

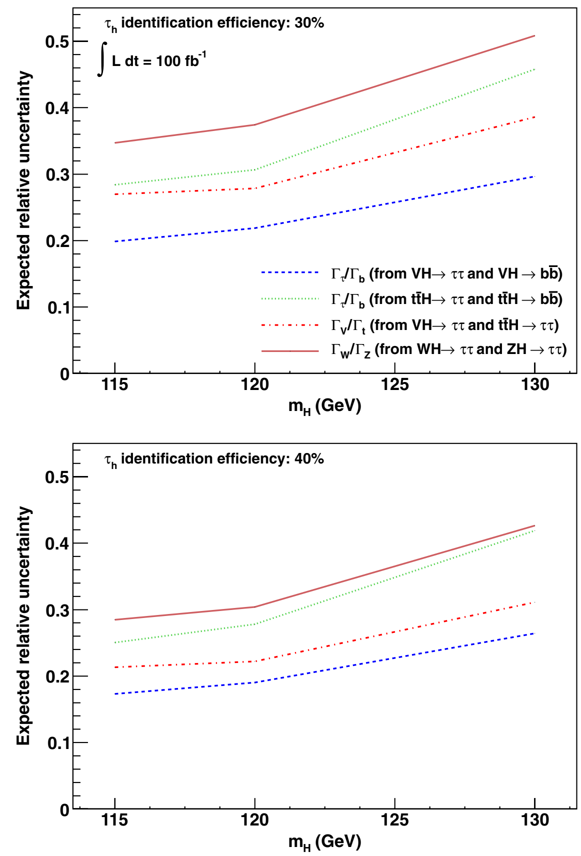

FIG. 5 (color online). The expected relative statistical uncertainties on ratios of partial widths using measurements of associated Higgs boson production and decays to tau-lepton or bottom-quark pairs. Each partial width Γ_i corresponds to the trilinear interaction of a Higgs boson to another particle i. Shown are the nominal (top) and optimistic (bottom) detector performance scenarios.

channels that have not been investigated in this context, or that have not been considered promising because of the expected large jet-to-τ background. Assuming the experiments can achieve similar tau reconstruction performance in $\sqrt{s} = 14$ TeV data as they have in $\sqrt{s} = 7$ TeV data, each experiment can measure the cross sections of WH and $t\bar{t}H$ production in the $H \rightarrow \tau\tau$ decay channels to $\approx$ 20% precision with 100 fb^{-1} of integrated luminosity. Additionally, with achievable $\not{p}_T$ reconstruction, a measurement of ZH production with an accuracy of $\approx$ 25% is possible with the same luminosity. With more data, the sensitivity to ZH and $t\bar{t}H$ production should improve, while sensitivity to WH production is unlikely to improve significantly due to systematic uncertainties on the background. If the assumed τ identification efficiency or $\not{p}_T$ resolution cannot be achieved, targeted background rejection through e.g. a multivariate analysis or improved mass reconstruction could compensate. Including additional decays of the tau leptons or top quarks would also improve sensitivity. By combining the associated production measurements in $H \rightarrow \tau\tau$ decays with measurements of the same production mechanisms in $H \to b\bar{b}$ decays [8–10], a precision of $\approx 20\%$ on the ratio of partial widths Γ_τ/Γ_b is achievable. We expect associated Higgs production with $H \to \tau\tau$ to provide an important contribution to Higgs coupling measurements with 100 fb^{-1} of integrated luminosity at $\sqrt{s} = 14$ TeV.

ACKNOWLEDGMENTS

This work was supported by the Science and Technology Facilities Council of the United Kingdom. C. H. would like to thank M. Mulhearn for discussions leading to the initial study of WH production.

[1] ATLAS Collaboration, Phys. Lett. B **716**, 1 (2012); CMS Collaboration, Phys. Lett. B **716**, 30 (2012).
[2] We use $c = 1$ here and subsequently.
[3] P. W. Higgs, Phys. Rev. Lett. **13**, 508 (1964); P. W. Higgs, Phys. Rev. **145**, 1156 (1966); F. Englert and R. Brout, Phys. Rev. Lett. **13**, 321 (1964); G. S. Guralnik, C. R. Hagen, and T. Kibble, Phys. Rev. Lett. **13**, 585 (1964); T. Kibble, Phys. Rev. **155**, 1554 (1967).
[4] http://lepewwg.web.cern.ch/LEPEWWG/
[5] The Tevatron Electroweak Working Group, arXiv:1204.0042v2; T. Aaltonen *et al.* (CDF Collaboration), Phys. Rev. Lett. **108**, 151803 (2012); V. M. Abazov *et al.* (DØ Collaboration), Phys. Rev. Lett. **108**, 151804 (2012); T. Aaltonen *et al.* (CDF Collaboration), Phys. Rev. D **77**, 112001 (2008).
[6] S. Schael *et al.* (ALEPH, DELPHI, L3, OPAL, and SLD Collaborations, LEP Electroweak Working Group, SLD Electroweak Group, and Heavy Flavor Groups), Phys. Rep. **427**, 257 (2006).
[7] The Tevatron Electroweak Working Group, arXiv:1107.5255v3.
[8] E. Richter-Was and M. Sapinski, Acta Phys. Pol. B **30**, 1001 (1999); V. Drollinger, T. Müller, and D. Denegri, arXiv:hep-ph/0111312v1.
[9] J. M. Butterworth, A. R. Davison, M. Rubin, and G. P. Salam, Phys. Rev. Lett. **100**, 242001 (2008); T. Plehn, G. P. Salam, and M. Spannowsky, Phys. Rev. Lett. **104**, 111801 (2010).
[10] K. Black *et al.*, J. High Energy Phys. 04 (2011) 069.
[11] E. Gabrielli, F. Maltoni, B. Mele, M. Moretti, F. Piccinini, and R. Pittau, Nucl. Phys. **781B**, 64 (2007).
[12] D. Zeppenfeld, R. Kinnunen, A. Nikitenko, and E. Richter-Was, Phys. Rev. D **62**, 013009 (2000).
[13] M. Duhrssen, S. Heinemeyer, H. Logan, D. Rainwater, G. Weiglein, and D. Zeppenfeld, Phys. Rev. D **70**, 113009 (2004).
[14] A. Djouadi, Phys. Rep. **457**, 1 (2008), and references therein.
[15] C. Boddy, Ph. D. thesis, Oxford University 2012; C. Boddy, S. Farrington, and C. Hays, Proc. Sci., ICHEP2010 (2010) 085.
[16] J. Gunion *et al.*, arXiv:hep-ph/9703330v2.
[17] CMS Collaboration, Report No. CMS-PAS-HIG-12-006 (2012).
[18] A. Belyaev and L. Reina, J. High Energy Phys. 08 (2002) 041.
[19] E. Gross and L. Zivkovic, Eur. Phys. J. C **59**, 731 (2009).
[20] ATLAS Collaboration, Report No. ATLAS-CONF-2011-152 (2011); CMS Collaboration, JINST **7**, P01001 (2012).
[21] J. Guasch, W. Hollik, S. Peñaranda, Phys. Lett. B **515**, 367 (2001).
[22] T. Gleisberg, S. Höche, F. Krauss, M. Schönherr, S. Schumann, F. Siegert, and J. Winter, J. High Energy Phys. 02, (2009) 007; We use version 1.2.1.
[23] M. L. Mangano, M. Moretti, F. Piccinini, R. Pittau, and A. Polosa, J. High Energy Phys. 07 (2003) 001.
[24] T. Sjöstrand, S. Mrenna, and P. Skands, J. High Energy Phys. 05 (2006) 026.
[25] S. Ovyn, X. Rouby, and V. Lemaitre, arXiv:0903.2225v3.
[26] ATLAS Collaboration, arXiv:0901.0512v4.
[27] CMS Collaboration, Report No. CERN/LHCC 2006-001, Vol. 1 (2006).
[28] J. Pumplin, D. R. Stump, J. Huston, H.-L. Lai, P. Nadolsky, and W.-K. Tung, J. High Energy Phys. 07 (2002) 012.
[29] M. Spira, http://people.web.psi.ch/spira/v2hv/.
[30] S. Dawson, C. Jackson, L. H. Orr, L. Reina, and D. Wackeroth, Phys. Rev. D **68**, 034022 (2003); W. Beenakker, S. Dittmaier, M. Krämer, B. Plümper, M. Spira, and P. M. Zerwas, Nucl. Phys. **653B**, 151 (2003); M. Spira, Fortschr. Phys. **46**, 203 (1998).
[31] A. Djouadi, J. Kalinowkski, and M. Spira, Comput. Phys. Commun. **108**, 56 (1998).
[32] O. Brein, A. Djouadi, and R. Harlander, Phys. Lett. B **579**, 149 (2004).
[33] M. L. Ciccolini, S. Dittmaier, and M. Krämer, Phys. Rev. D **68**, 073003 (2003).
[34] J. M. Campbell and R. K. Ellis, Phys. Rev. D **60**, 113006 (1999).
[35] M. Cacciari, S. Frixione, M. L. Mangano, P. Nason, and G. Ridolfi, J. High Energy Phys. 09 (2008) 127.
[36] K. Nakamura *et al.* (Particle Data Group), J. Phys. G **37**, 075021 (2010).
[37] A. Lazopoulos, T. McElmurry, K. Melnikov, and F. Petriello, Phys. Lett. B **666**, 62 (2008).
[38] CMS Collaboration, arXiv:1206.4071v1.
[39] M. Cacciari, G. P. Salam, and G. Soyez, J. High Energy Phys. 04 (2008) 063.